MODELING OF FRAGMENT LOADS AND EFFECTS ON REINFORCED CONCRETE SLABS

L. Javier Malvar
James W. Wesevich
John E. Crawford
Karagozian and Case Structural Engineers
625 North Maryland Avenue
Glendale, CA 91206-2245
(818) 240-1919

ABSTRACT

This paper describes a technique used to characterize the loading and damage generated by the primary fragments from cased munitions on reinforced concrete slabs or walls. It has been observed that the damage generated by the fragments, while usually of secondary importance to the airblast, can in some circumstances dominate the response. Test observations indicate that fragments from cased conventional bombs, not only directly load a wall element through momentum transfer, but also create a substantial amount of damage on the wall's front face. This damage may include slicing of the reinforcement and complete removal of concrete from the front face to depths beyond the front face reinforcement. Single fragment tests have also shown that the momentum transferred is substantially greater than the fragment momentum prior to impact, due to the significant amount of concrete debris ejected from the impact crater. Equivalent forcing functions, in terms of pressure versus time, are derived to approximate both the momentum transfer and the damage generated in the concrete. The calculations used to demonstrate these techniques were performed with the three-dimensional Lagrangian finite element code DYNA3D and a specially modified concrete model which includes the effects of fracture, fracture energy based strain softening, and strain rate.

FRAGMENT IMPACT TESTS

Figure 1 depicts the type and extent of damage that can occur to a reinforced concrete slab from the fragments generated by a cased bomb. Measurements of the crater depths are given in Figure 2.

In tests to measure the effect of single fragments on reinforced concrete slabs, it was observed that the fragment would create a crater in the slab with a significant amount of concrete being ejected from the impact crater; much of the ejecta traveled in a direction normal to the slab (*i.e.*, in the direction opposite that of the fragment). As a consequence, the amount of impulse transmitted to the slab was greater than the initial fragment momentum (*i.e.*, fragment plus ejecta momentum). Transmitted impulses of nearly twice the initial fragment momentum have been observed.

Report Documentation Page

Form Approved
OMB No. 0704-0188

1. REPORT DATE	2. REPORT TYPE	3. DATES COVERED
AUG 1996		**00-00-1996 to 00-00-1996**

4. TITLE AND SUBTITLE	5a. CONTRACT NUMBER
Modeling of Fragment Loads and Effects on Reinforced Concrete Slabs	5b. GRANT NUMBER
	5c. PROGRAM ELEMENT NUMBER
6. AUTHOR(S)	5d. PROJECT NUMBER
	5e. TASK NUMBER
	5f. WORK UNIT NUMBER
7. PERFORMING ORGANIZATION NAME(S) AND ADDRESS(ES) **Karagozian and Case Structural Engineers,625 North Maryland Avenue,Glendale,CA,91206-2245**	8. PERFORMING ORGANIZATION REPORT NUMBER
9. SPONSORING/MONITORING AGENCY NAME(S) AND ADDRESS(ES)	10. SPONSOR/MONITOR'S ACRONYM(S)
	11. SPONSOR/MONITOR'S REPORT NUMBER(S)

12. DISTRIBUTION/AVAILABILITY STATEMENT
Approved for public release; distribution unlimited

13. SUPPLEMENTARY NOTES
See also ADM000767. Proceedings of the Twenty-Seventh DoD Explosives Safety Seminar Held in Las Vegas, NV on 22-26 August 1996.

14. ABSTRACT
see report

15. SUBJECT TERMS

16. SECURITY CLASSIFICATION OF:			17. LIMITATION OF ABSTRACT	18. NUMBER OF PAGES	19a. NAME OF RESPONSIBLE PERSON
a. REPORT	b. ABSTRACT	c. THIS PAGE			
unclassified	**unclassified**	**unclassified**	**Same as Report (SAR)**	**11**	

Figure 1. Pictures of fragment damage of a reinforced concrete slab caused by a cased munition.

FINITE ELEMENT ANALYSIS

The Lagrangian, explicit finite element program DYNA3D [1] was used for the analyses. Explicit time integration allows for very fine discretizations and the modeling of highly transient loads. Two mesh sizes—0.5 and 1 inch—were used to evaluate mesh sensitivity of the damage prediction, Figures 3 through 5. If the mesh size is too large, the effect of a single fragment impact cannot be captured. Three-dimensional solid elements were used for the concrete, and discrete beam elements modeled the rebar.

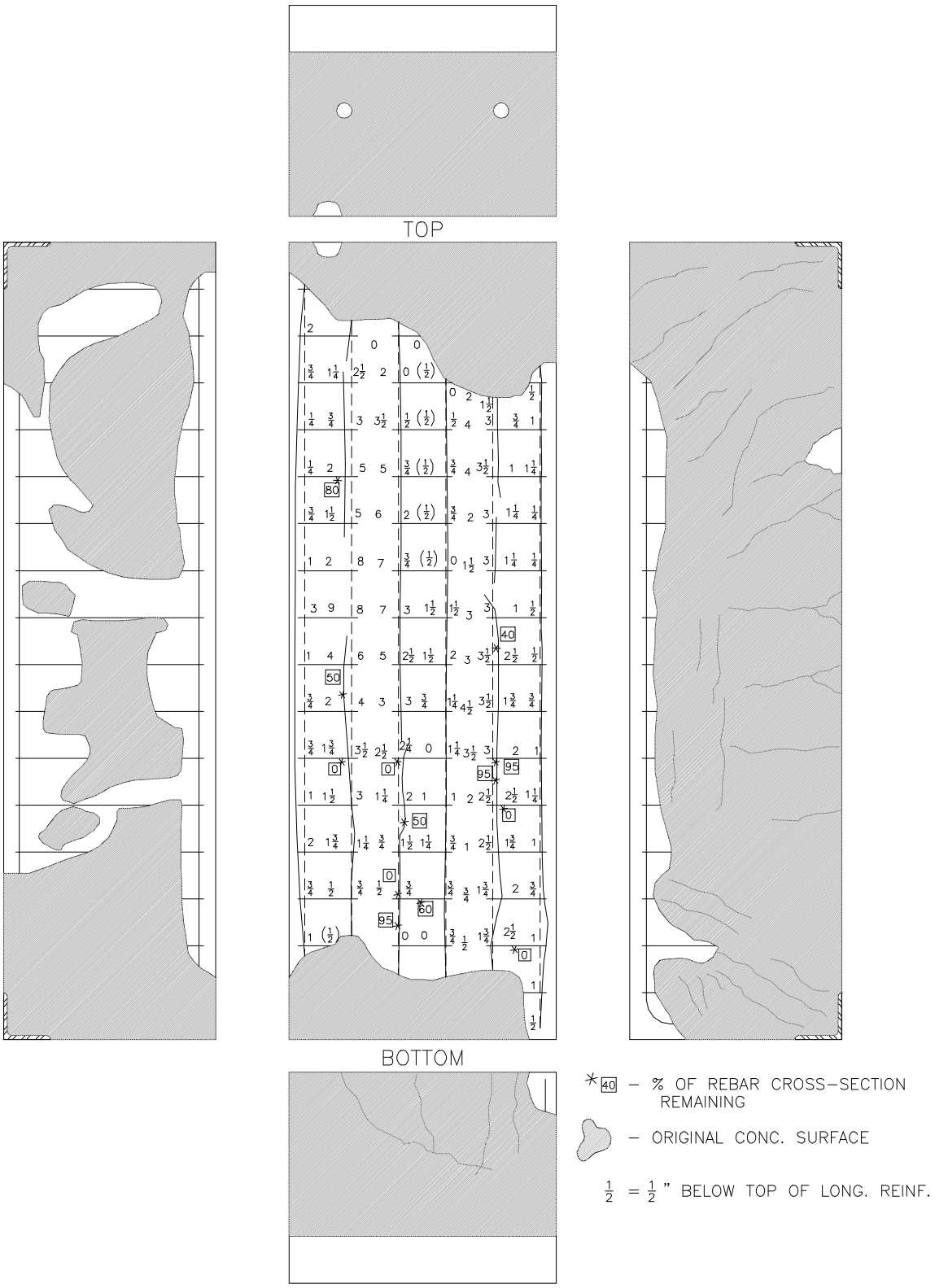

Figure 2. Quantitative measure of fragment damage.

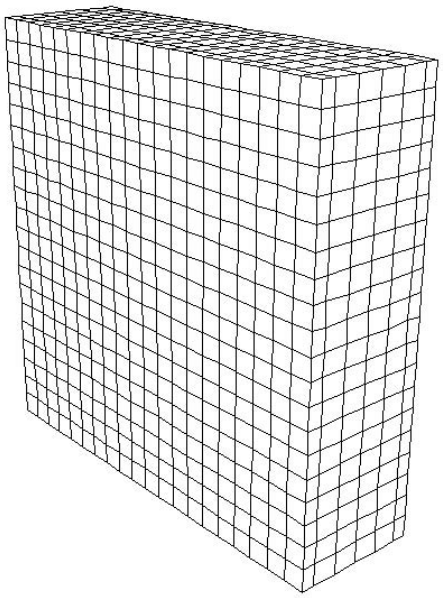

Figure 3. Undamaged 1-inch model.

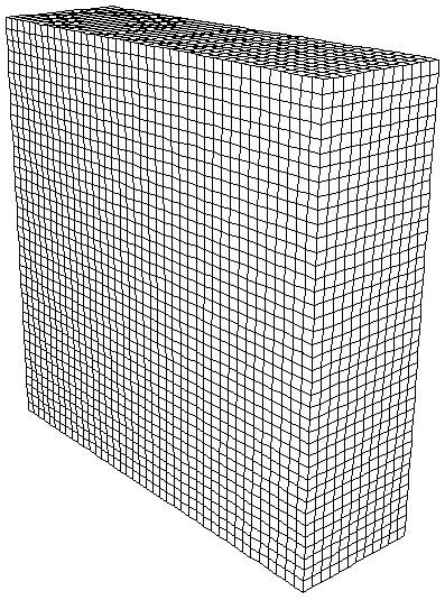

Figure 4. Undamaged 0.5-inch model.

MATERIAL MODELS

The nominal concrete strength used in this study is 5,000 psi. The material model used to model the concrete in this study is a highly modified version of the DYNA3D Material 16. The modifications made to Material 16 include the following: (1) a three-invariant formulation in compression; (2) an enhanced failure surface in tension; (3) more consistent failure for uniaxial, biaxial, triaxial tensile tests, pure shear test, and uniaxial and biaxial compression tests; and (4) a corrected strain rate enhancement for both tension and compression. A damage measure which is a function of the effective plastic strain controls the material model's damage evolution. Documentation for these enhancements may be found in References 3-5.

The steel reinforcing bars were discretely modeled; each bar was modeled using a truss/beam element placed at the corresponding location. The material model used for the steel rebar (Material 19—strain rate dependent isotropic elastic plastic) was modified to include a smooth stress-strain relationship and a rupture strain [7]. The yield stress was 60 ksi, and the ultimate strength was 87 ksi.

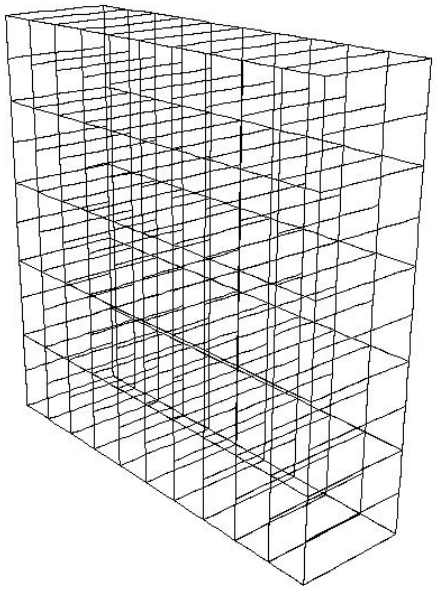

Figure 5. Typical reinforcement layout.

FRAGMENT IMPULSE

A pressure history derived from the measurements of the momentum transferred to a reinforced concrete slab by a single fragment is shown in Figure 6. The impulse of this load (*i.e.*, 24 psi-sec) is equivalent to the total impulse applied to the slab (*i.e.*, nearly two times the fragment's momentum) over a time period consistent with the observed data.

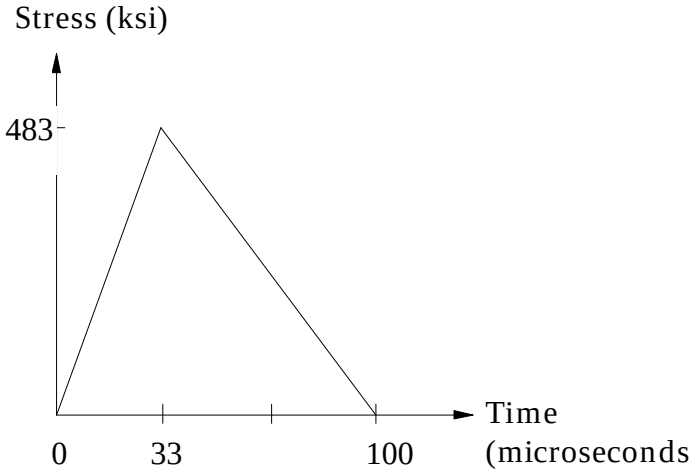

Figure 6. Pressure history equivalent of fragment loading.

RESULTS

Figure 7 shows a contour of the damage accumulated in the slab by 10 ms. This plot indicates the final shape of the impact crater. Figures 8 through 16 show contours of pressure, damage, and velocity at 10 μs intervals from 10 to 120 μs.

Assessment of Shock Wave Propagation via Pressure Plots

Figures 8 through 10 show pressure contours which capture the shock wave traveling through wall (including reversal from compression to tension upon reflection off the back face). Starting at about 33 μs (peak input pressure) it takes about 75 μs for the initial two-way passage.

Assessment of Shock Wave Propagation via Damage Plots

Upon arrival of the load, the concrete slab initially deforms elastically. Plastic damage starts accumulating only after 20 μs with pronounced softening occurring after 30 μs, as shown in Figures 11 through 13. The damage keeps increasing until the compression wave decays enough so that only elastic deformation is present. Hence no increase in plastic damage is seen after about 60 μs. Additional damage is seen again upon arrival of the reflected tension wave (after 90 μs). This implies a dependency of the damage on the time history applied and on the slab thickness.

Assessment of Shock Wave Propagation via Velocity Plots

Velocity contours follow the compression wave. The velocity is almost uniform (rigid body motion) as soon as the loading phase has been completed (after 100 μs), see Figures 14 through 16.

Momentum Deposition versus Observed Damage

Using momentum deposition nearly twice the fragment momentum produces a crater consistent with those observed in single fragment tests.

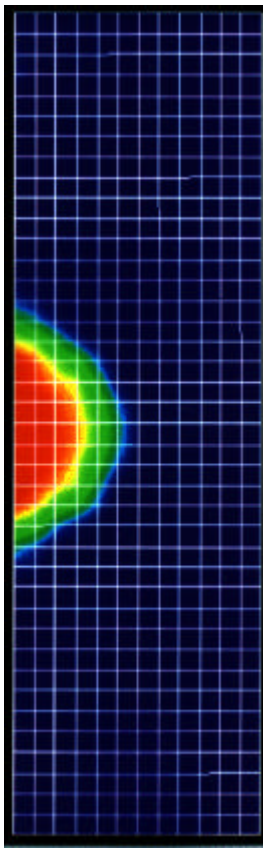

Figure 7. Damage fringe plot at 10 ms.

CONCLUSION

For the concrete constitutive model used in this paper, proper modeling of fragment impact is obtained, at least qualitatively, if momentum deposition of approximately twice that of the fragment momentum is used to generate an equivalent pressure-history, which is to be applied to the face of the undamaged slab over an area equivalent to the area of the fragment.

REFERENCES

1. Whirley, R. G. and B. E. Engelmann, “DYNA3D: A Nonlinear Explicit Three-Dimensional Finite Element Code for Solid and Structural Mechanics,” User Manual, Report UCRL-MA-107254 Rev. 1, Lawrence Livermore National Laboratory, Livermore, CA, November 1993.

2. Wesevich, J. W., L. J. Malvar, J. E. Crawford, “Calculation Results: Fragment Test No. 28,” Proceedings, Defense Nuclear Agency Airblast and Structural Calculations Meeting, Logicon RDA, Albuquerque, NM, February 28, 1996.

3. Malvar, L. J. and D. Simons, “Concrete Material Modeling in Explicit Computations,” Proceedings, Workshop on Recent Advances in Computational Structural Dynamics and High Performance Computing, USAE Waterways Experiment Station, Vicksburg, MS, April 1996, pp. 165-194.

4. Malvar, L. J., J. E. Crawford, J. W. Wesevich, D. Simons, "A New Concrete Material Model for DYNA3D - Release II: Shear Dilation and Directional Rate Enhancements," TM-96-2.1, Report to the Defense Nuclear Agency, Karagozian and Case Structural Engineers, Glendale, CA, January 1996.

5. Malvar, L. J., J. Crawford, D. Simons, J. W. Wesevich, “A New Concrete Material Model for DYNA3D,” Proceedings, 10th ASCE Engineering Mechanics Conference, Vol. 1, Boulder, CO, May 1995, pp. 142-146.

6. Malvar, L. J., J. E.Crawford, J. W.Wesevich, D. Simons, "A New Concrete Material Model for DYNA3D," TM-94-14.3, Report to the Defense Nuclear Agency, Karagozian and Case Structural Engineers, Glendale, CA, October 1994.

7. Pelessone, D. and C. Charman, 1992. "User's Manual Supplement for DNA Version of the DYNA3D Code," GA-C20983, General Atomics, San Diego, CA.

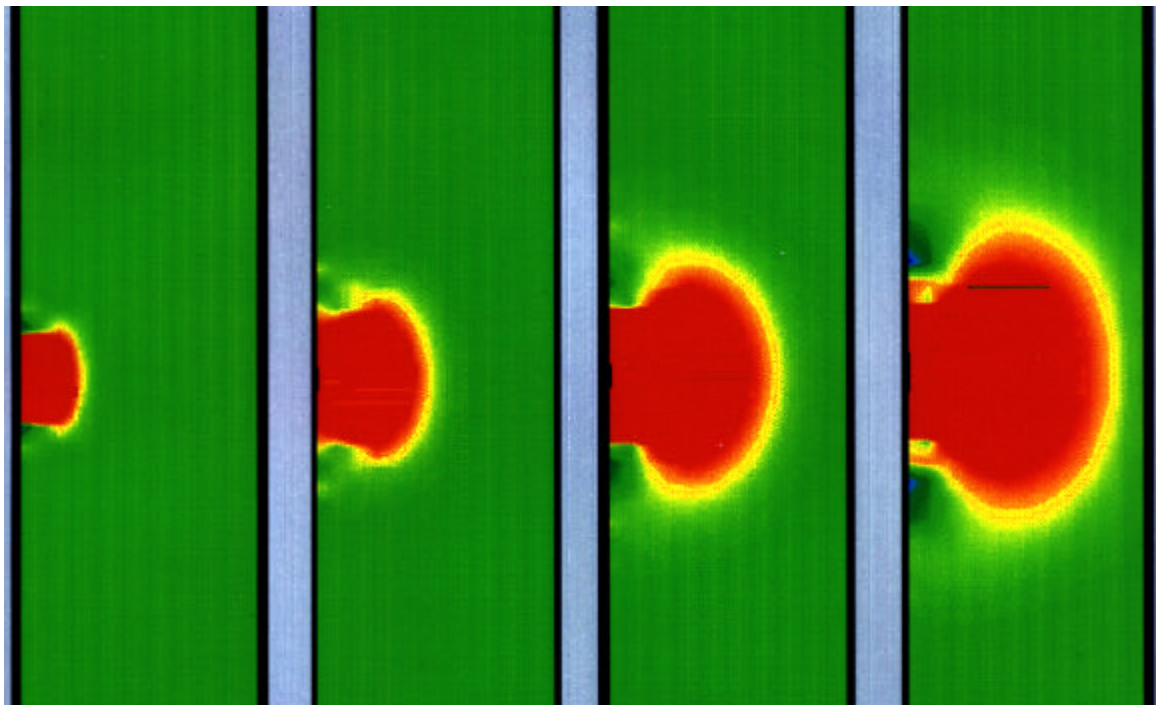

(a) 10 μs. (b) 20 μs. (c) 30 μs. (d) 40 μs.

Figure8. Pressure fringe plots from 10-40 μs.

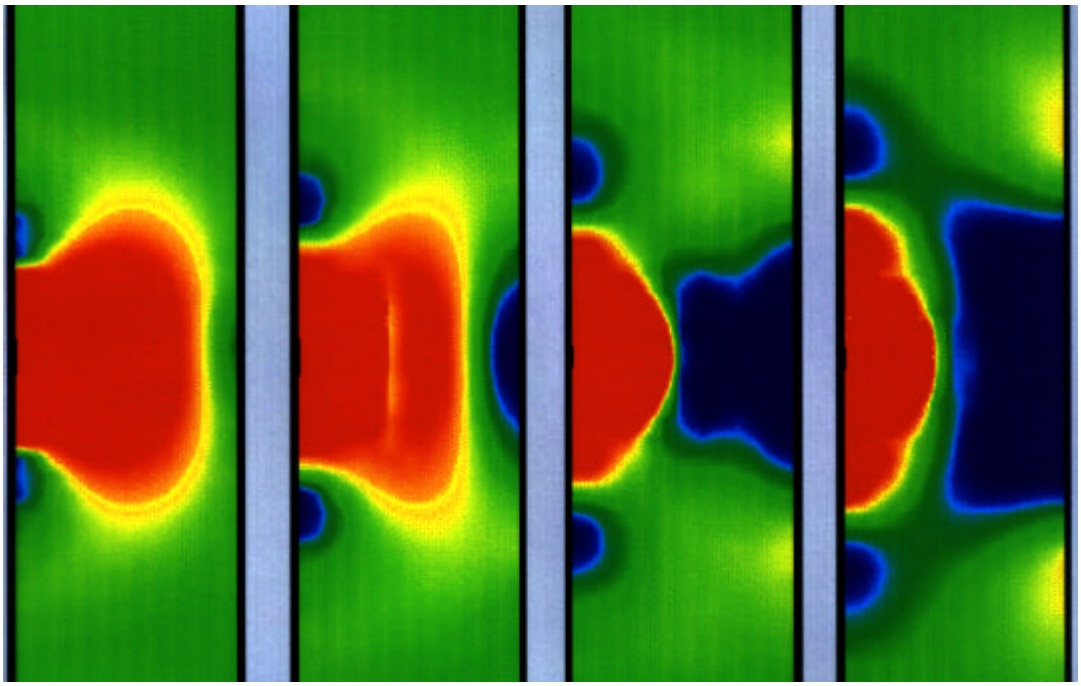

(a) 50 μs. (b) 60 μs. (c) 70 μs. (d) 80 μs.

Figure 9. Pressure fringe plots from 50-80 μs.

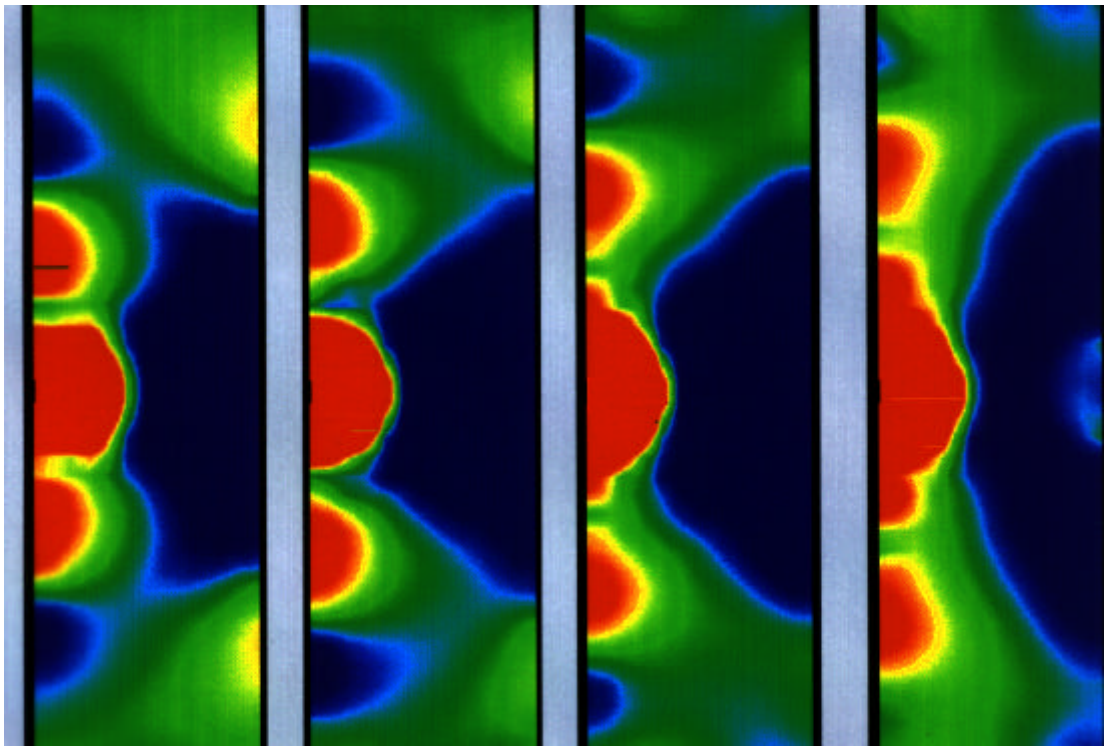

(a) 90 μs. (b) 100 μs. (c) 110 μs. (d) 120 μs.

Figure 10. Pressure fringe plots from 90-120.

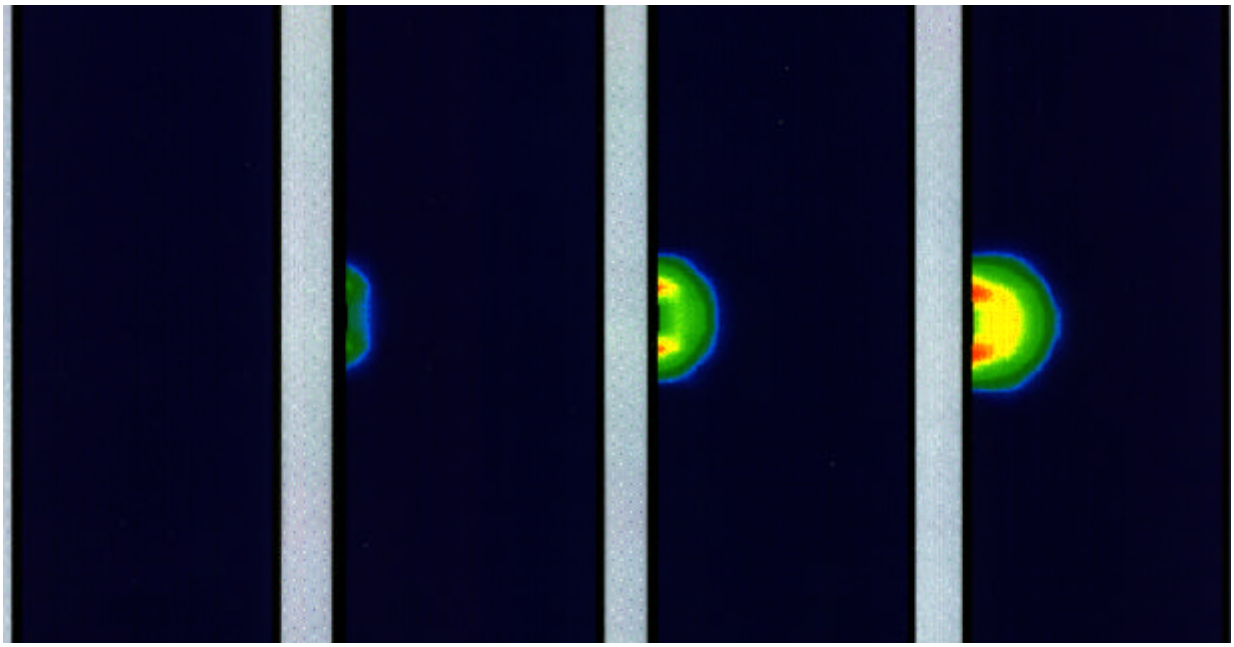

(a) 10 μs. (b) 20 μs. (c) 30 μs. (d) 40 μs.

Figure 11. Damage fringe plots from 10-40 μs.

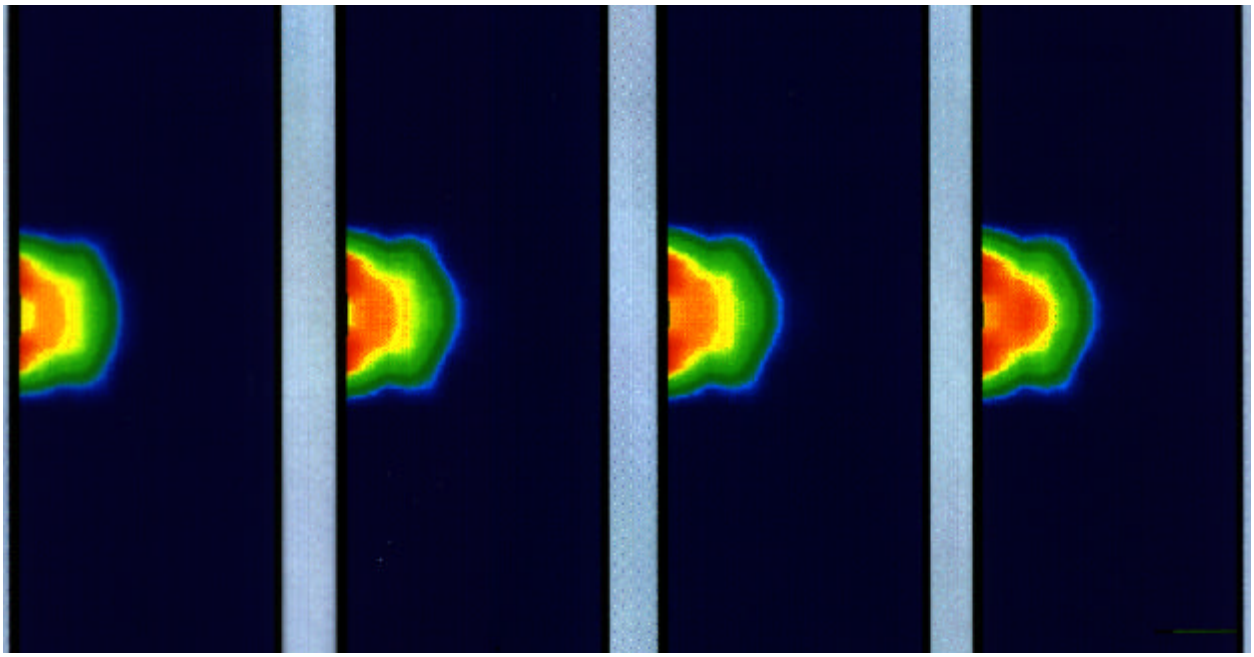

(a) 50 μs. (b) 60 μs. (c) 70 μs. (d) 80 μs.

Figure 12. Damage fringe plots from 50-80 μs.

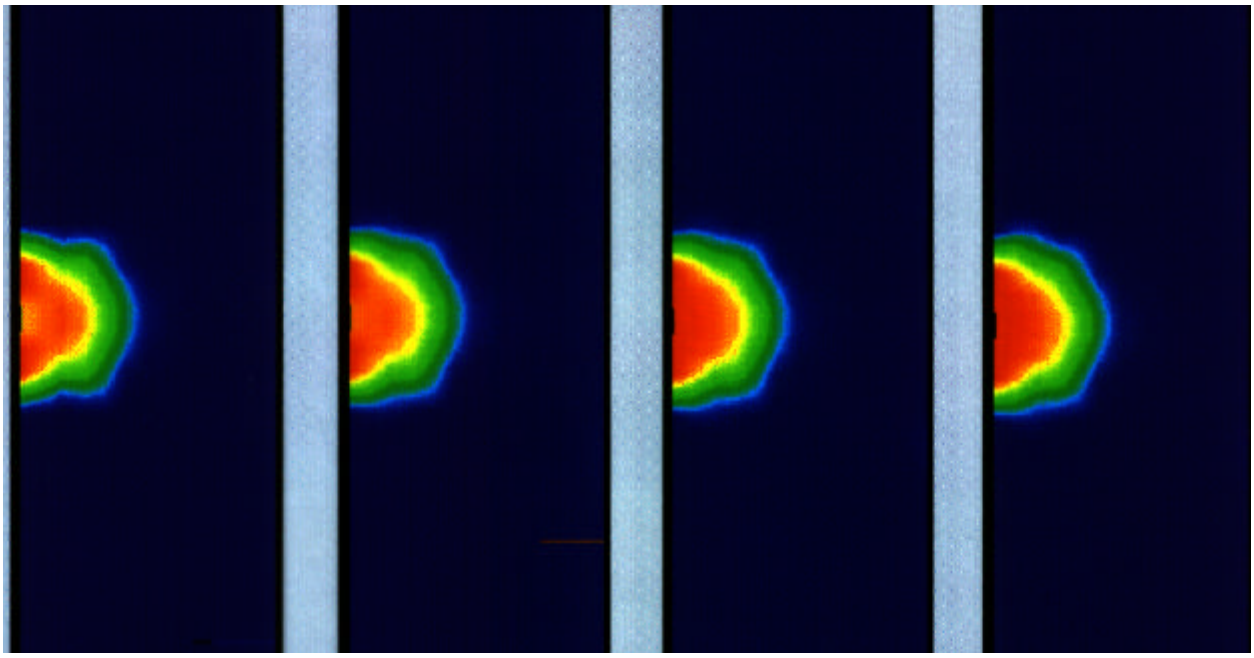

(a) 90 μs. (b) 100 μs. (c) 110 μs. (d) 120 μs.

Figure 13. Damage fringe plots from 90-120 μs.

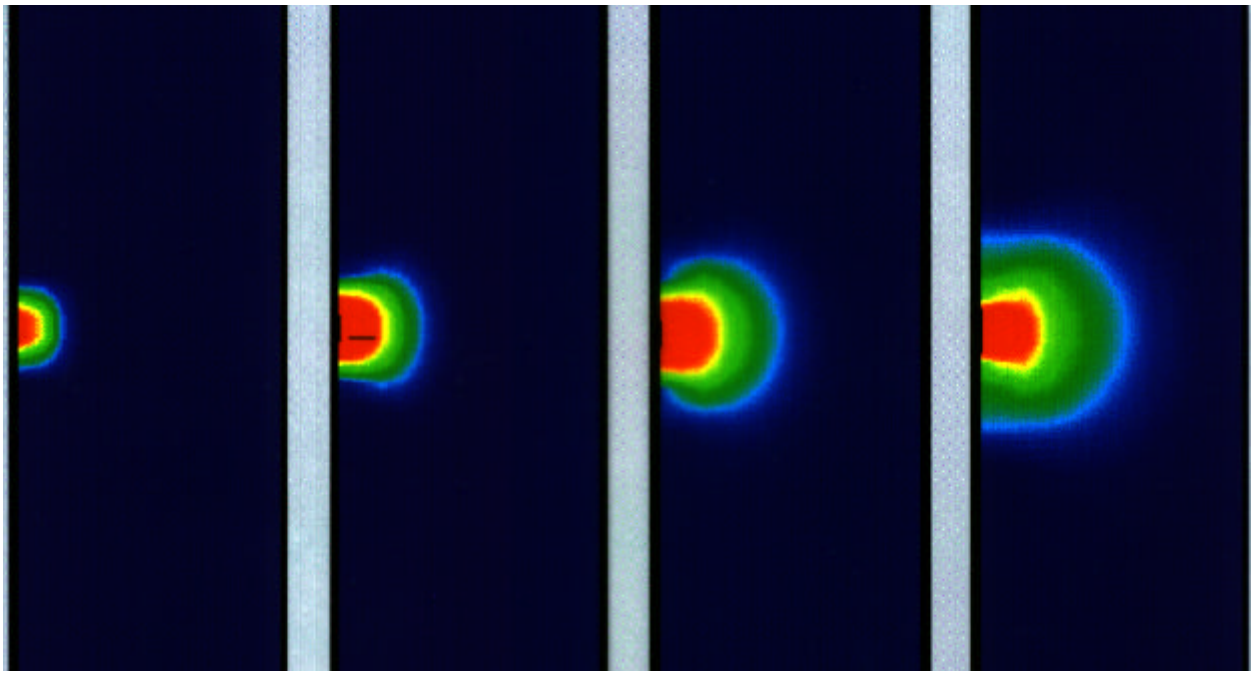

(a) 10 μs. (b) 20 μs. (c) 30 μs. (d) 40 μs.

Figure 14. Resultant velocity fringe plots from 10-40 μs.

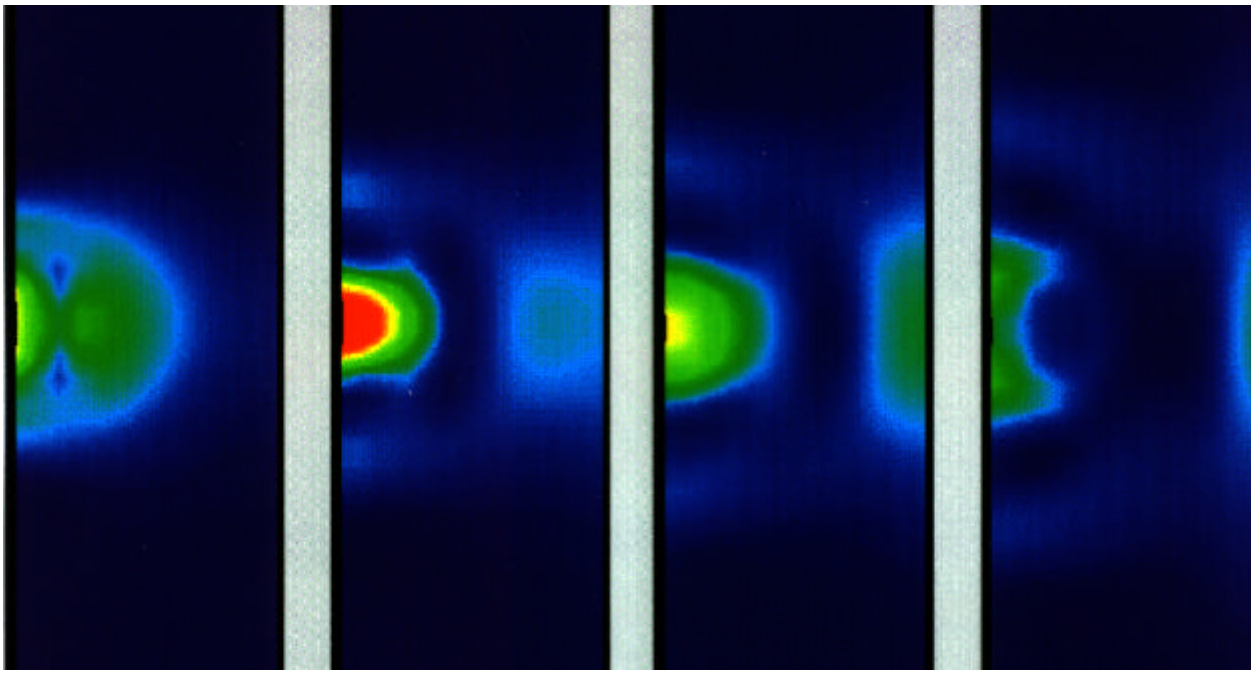

(a) 50 μs. (b) 60 μs. (c) 70 μs. (d) 80 μs.

Figure 15. Resultant velocity fringe plots from 50-80 μs.

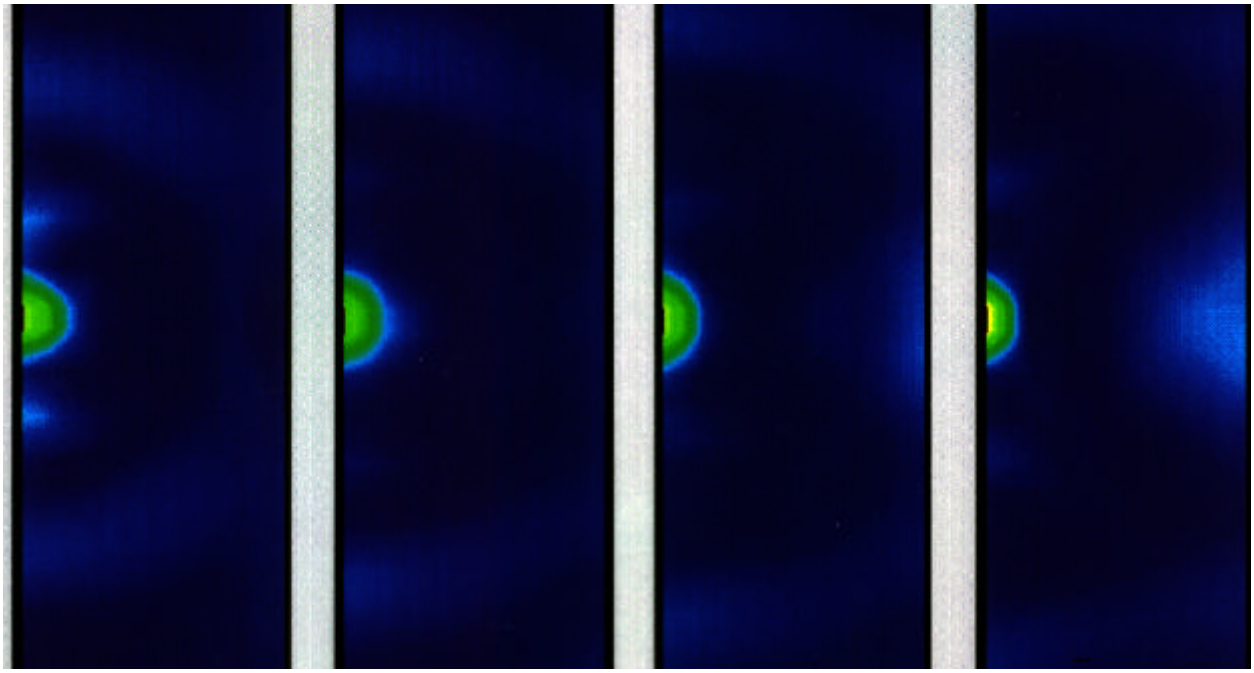

(a) 90 μs. (b) 100 μs. (c) 110 μs. (d) 120 μs.

Figure 16. Resultant velocity fringe plots from 90-120 μs.